

ARTICLE OPEN

Synthetic macrolides overcoming MLS_BK-resistant pathogens

Cong-Xuan Ma^{1,6}, Ye Li^{2,3,6}, Wen-Tian Liu¹, Yun Li⁴, Fei Zhao⁵, Xiao-Tian Lian¹, Jing Ding¹, Si-Meng Liu¹, Xie-Peng Liu¹, Bing-Zhi Fan¹, Li-Yong Liu⁵, Feng Xue⁴, Jian Li^{2,3}, Jue-Ru Zhang¹, Zhao Xue^{2,3}, Xiao-Tong Pei^{2,3}, Jin-Zhong Lin¹ and Jian-Hua Liang¹

© The Author(s) 2024

Conventional macrolide-lincosamide-streptogramin B-ketolide (MLS_BK) antibiotics are unable to counter the growing challenge of antibiotic resistance that is conferred by the constitutive methylation of rRNA base A2058 or its G2058 mutation, while the presence of unmodified A2058 is crucial for high selectivity of traditional MLS_BK in targeting pathogens over human cells. The absence of effective modes of action reinforces the prevailing belief that constitutively antibiotic-resistant *Staphylococcus aureus* remains impervious to existing macrolides including telithromycin. Here, we report the design and synthesis of a novel series of macrolides, featuring the strategic fusion of ketolide and quinolone moieties. Our effort led to the discovery of two potent compounds, MCX-219 and MCX-190, demonstrating enhanced antibacterial efficacy against a broad spectrum of formidable pathogens, including A2058-methylated *Staphylococcus aureus*, *Streptococcus pneumoniae*, *Streptococcus pyogenes*, and notably, the clinical *Mycoplasma pneumoniae* isolates harboring A2058G mutations which are implicated in the recent pneumonia outbreak in China. Mechanistic studies reveal that the modified quinolone moiety of MCX-190 establishes a distinctive secondary binding site within the nascent peptide exit tunnel. Structure-activity relationship analysis underscores the importance of this secondary binding, maintained by a sandwich-like π - π stacking interaction and a water-magnesium bridge, for effective engagement with A2058-methylated ribosomes rather than topoisomerases targeted by quinolone antibiotics. Our findings not only highlight MCX-219 and MCX-190 as promising candidates for next-generation MLS_BK antibiotics to combat antibiotic resistance, but also pave the way for the future rational design of the class of MLS_BK antibiotics, offering a strategic framework to overcome the challenges posed by escalating antibiotic resistance.

Cell Discovery; <https://doi.org/10.1038/s41421-024-00702-y>

INTRODUCTION

The bacterial 70S ribosome serves as the universal translator for protein synthesis and is a vital target for antibacterial agents. This is because more than half of antibiotics bind to different sites on the ribosome, thereby selectively disrupting the process of protein synthesis^{1,2}. The World Health Organization has identified twelve lethal pathogenic species, including methicillin-resistant *Staphylococcus aureus* (MRSA), penicillin-resistant *Streptococcus pneumoniae* and ampicillin-resistant *Haemophilus influenzae*, as high- to medium-priority resistant bacteria which require immediate attention. Macrolide-lincosamide-streptogramin B (MLS_B), one of the most successful classes of antibiotics, was widely prescribed to treat infections caused by those pathogens. However, multi-drug-resistant pathogens pose a significant threat to human health and reduce the effectiveness of currently available MLS_B antibiotics^{3–6}.

Structurally unrelated MLS_B antibiotics are positioned at the narrowest site within the nascent peptide exit tunnel (NPET) of the ribosome, close to the catalytic peptidyl transferase center (PTC). Clinically, it is observed that alteration of bacterial ribosomal RNA (rRNA) bases renders bacteria insensitive to the available arsenal of ribosome-targeting antibiotics. It has been clarified that the

most prevalent mechanism of cross-resistance to MLS_B is mono- or di-methylation of the N6 position of rRNA base A2058 (*Escherichia coli* numbering is used throughout the text unless concurrent *S. aureus* numbering indicated in parentheses), which is catalyzed by erm-mediated methyltransferases^{7,8}. In contrast to the low-level efflux resistance encoded by *mef* genes, methylation at A2058 and mutation of A2058 can lead to high-level antibiotic resistance, either induced by erythromycin (inducible phenotype) or occurring in the absence of erythromycin (constitutive phenotype).

Resistance to MRSA is often associated with constitutive phenotypes of MLS_B rather than inducible phenotypes of MLS_B⁹, necessitating the development of new MLS_B actively against constitutive resistance. Nevertheless, there is a long-standing notion that constitutively resistant *S. aureus* cannot be effectively overcome by currently available macrolides, which was first claimed by scientists at Pfizer in 2007^{9–11}. To revitalize MLS_B, unnatural MLS_B scaffolds which are not accessible by semisynthetic method, approaches have been constructed through a convergent and efficient total synthesis method that enables the synthesis of diverse structures^{12–14}. The availability of unnatural scaffolds significantly expands the chemical space for drug design

¹Key Laboratory of Medicinal Molecule Science and Pharmaceutical Engineering, School of Chemistry and Chemical Engineering, Beijing Institute of Technology, Beijing, China.

²State Key Laboratory of Genetic Engineering, School of Life Sciences, Zhongshan Hospital, Fudan University, Shanghai, China. ³Center for mRNA Translational Research, Fudan University, Shanghai, China. ⁴Institute of Clinical Pharmacology, Peking University First Hospital, Beijing, China. ⁵National Institute for Communicable Disease Control and Prevention, Chinese Center for Disease Control and Prevention, State Key Laboratory of Infectious Disease Prevention and Control, Beijing, China. ⁶These authors contributed equally: Cong-Xuan Ma, Ye Li. ✉email: linjinzhong@fudan.edu.cn; ljhbit@bit.edu.cn

Received: 18 April 2024 Accepted: 26 June 2024

Published online: 11 July 2024

of newer MLS_B. However, the optimized macrolides, regardless of their varying macrolactone ring sizes, still demonstrate inactivity against constitutively A2058-methylated *S. aureus*¹². Recently, cresomycin, a novel lincosamide with an additional isobutyl substituent, restored activity against A2058-methylated *S. aureus* by extending the isobutyl substituent to the A-site of PTC and disrupting translation initiation¹⁴. On the other hand, infections caused by MLS_B-resistant *Mycoplasma pneumoniae*, occurring both endemically and epidemically worldwide, have received less attention^{3,15}. *M. pneumoniae* is a unique bacterium as it lacks a cell wall, making it resistant to certain antibiotics that target cell walls. In 2023, the prevalence of azithromycin-resistant *M. pneumoniae* as a first-line treatment challenge has led to an extended outbreak among children in China, primarily due to the lack of safe and efficacious antibiotics for combating the infection. Notably, *M. pneumoniae*, which carries a single chromosomal rRNA operon (in contrast to six *rrn* alleles in the conventional *S. aureus* strains), exhibits resistance to the first-, second-, and third-generation macrolides currently available in the market (such as erythromycin, clarithromycin/azithromycin and telithromycin, respectively, Fig. 1a) by the G2058 mutation in rRNA¹⁵. Intriguingly, eukaryotic ribosomes have a conserved G2058 at the equivalent position, serving as a determinant contributing to the selective action of MLS_B antibiotics on bacterial ribosomes¹⁶. Thus far, A2058-modified MLS_B resistance remains a great challenge for the development of the next generation of MLS_B.

Macrolides, consisting of a 14–16 membered macrolactone and several sugars, are best represented by erythromycin, which has been safely used for more than 70 years to treat community-acquired or hospital-acquired respiratory tract infections caused by *S. aureus*, *S. pneumoniae*, *Streptococcus pyogenes*, *M. pneumoniae*, *H. influenzae* and *Moraxella catarrhalis*. The prevalence of resistance has been exacerbated by the second-generation cladinose-containing erythromycins, such as clarithromycin and 15-membered azithromycin. To address the issue of cladinose-induced A2058 methylation and efflux resistance, a direct approach comprises eliminating the C-3 cladinose and introducing a validated non-inducible group^{17–21}. Telithromycin and its analog solithromycin, the representative ketolides structurally characterized by the 3-ketone and additional alkyl-aryl arms extending from the 11, 12-position of the lactone, demonstrate potency against constitutively methylated strains of *S. pneumoniae* and *S. pyogenes* by providing an additional π - π contact with rRNA base pair A752–U2609^{22–24}. Nevertheless, a comparative analysis of the structure of telithromycin in complex with the *S. aureus* ribosome revealed that the aryl group anchored at the end of the side chain of telithromycin is unable to interact with rRNA bases of *S. aureus*, rationalizing the observed ineffectiveness of macrolides against constitutively methylated *S. aureus*²⁵. Notably, the development of ketolides is hindered by unfavorable impacts, such as liver damage, named the Ketek (telithromycin) effect, as well as the weak inducer due to a ribosomal frameshifting mechanism²⁶. Moreover, a significant proportion of these ketolide-sensitive *S. pyogenes* and *S. pneumoniae* remains rRNA A2058-monomethylated, and the inducer would further increase the proportion of dimethylated A2058 ribosomes, which confers high resistance to ketolides²⁷. This highlights the difficulties in developing effective strategies to address MLS_BK resistance²⁸.

Hybridizing two pharmacophores is a promising therapeutic strategy in drug discovery and several hybrids are under clinical evaluation^{29,30}. Initially, attaching the fluoroquinolone element to the 4"-position of C-3 cladinose of macrolides was developed by ref. 31. Thus, many so-called macrolones (a hybrid of the macrolide and the quinolone, mostly characterized with an extended linker originating from the cladinose) have been extensively investigated^{11,28,31–44}. Thus far, only one of the C-6-derived 15-membered macrolones has shown moderate activity against an isolate of constitutively MLS_B-resistant but quinolone-sensitive

*S. aureus*¹¹. Nonetheless, it remains unclear whether its antibacterial mechanism involves action on topoisomerase⁴³, especially given that the tested strain is sensitive to quinolones, and no further biological analysis on potential targets has been provided. Hence, the approach to improve the efficacy of macrolones in inhibiting A2058-modified *S. aureus* and *M. pneumoniae* cell growth remains unidentified.

In this work, we have synthesized a novel class of synthetic macrolides, representing a unique hybridization of ketolide and quinolone moieties. The lead compounds, MCX-219 and MCX-190, featuring a modified quinolone motif and an effective hybrid approach, demonstrate a revived antibacterial spectrum against a range of microorganisms resistant to MLS_BK, including *S. aureus*, *S. pneumoniae*, *S. pyogenes*, and *M. pneumoniae*, as well as the Gram-negative *H. influenzae* and *M. catarrhalis*. We provide structural and biochemical evidence that elucidates the mechanisms underpinning the robust and extensive antibacterial activity of these newly developed macrolides, specifically targeting the A2058-modified ribosome in a manner that bears resemblance to targeting topoisomerase. This discovery would be instrumental in formulating the other MLS_BK antibiotics.

RESULT

Discovery of MCX-219 and MCX-190 guided by structure-activity relationships (SARs)

The known SARs of macrolones exhibit notable distinctions from those of quinolones targeting topoisomerases. For example, a majority of macrolones are consistently constructed by linking through the C-4"-position of the macrolide and the C-6-position of the quinolone nucleus because slightly favorable effects on activity were observed when substituting positions shifted from C-7 to C-6 of quinolones^{34,37,39–41}. Moreover, 3-esterification of quinolone in macrolones resulted in an acceptable increase in minimum inhibitory concentrations (MICs)^{34,36,38}. In contrast, this work underscores the significance of substituting the linker at the C-7 position of quinolones (57c vs 57a, 61c vs 61a) and maintaining the original chemotype of 3-carboxylic acid of quinolones (88h vs 88g, 61c vs 61d), as shown in Fig. 1c. This disparity can be attributed to the limited knowledge of SARs when a quinolone is attached to the 3-O position of 3-O-descladinose macrolides. Therefore, the SARs discovered in this work differ significantly from those of macrolones but share similarities with the established SARs of quinolones. Additionally, a comparison of the rigid alkyl linker in 57c vs the flexible alkyl linker in 61c demonstrates the favorability of the rigid linker in enhancing activity against fastidious *H. influenzae*.

Further exploration into varying functionality at the 9- or/and 11-positions (57c vs 79c vs 87c), varying linkers' length (87c vs 88c, 88g vs 89g, 95g vs 96g), and the insertion of heteroatoms such as oxygen or nitrogen atoms into the linkers connecting macrolides to quinolones (71c vs 72c, 88g vs 95g, 89g vs 96g, 95c vs 98c) was performed, as detailed in Fig. 1c. Among the hybrids, compound 88g, characterized by 11,12-cyclic carbamate, 9-keto functionality, and the introduction of a new spacer of octynyl carbamate at C-3, exhibited the highest activity against constitutively MLS_BK-resistant *S. pneumoniae*, *S. pyogenes*, and *S. aureus*.

The significantly increased MICs of 95j and 88j possessing 3-quinolylcarboxylic acid emphasized the importance of the C-4 ketone of quinolones, as shown in Fig. 1c. Further exploration of quinolone-like scaffolds, such as quinazolin-4(3H)-one and 1,3-dihydroxyxanthone proved unsuccessful, indicating the importance of quinolones (88g vs 88j, 88l and 88m). However, varying groups at N-1 of quinolones, such as H atom, or methyl, ethyl, and bulky cyclic propyl groups (88c vs 88g, 95c, 95f, and 95g vs 95i), indicated that the sterically smaller methyl group at N-1 is the best substituent for improving activities (88g and 95g, Fig. 1c), which is different from the established SARs for

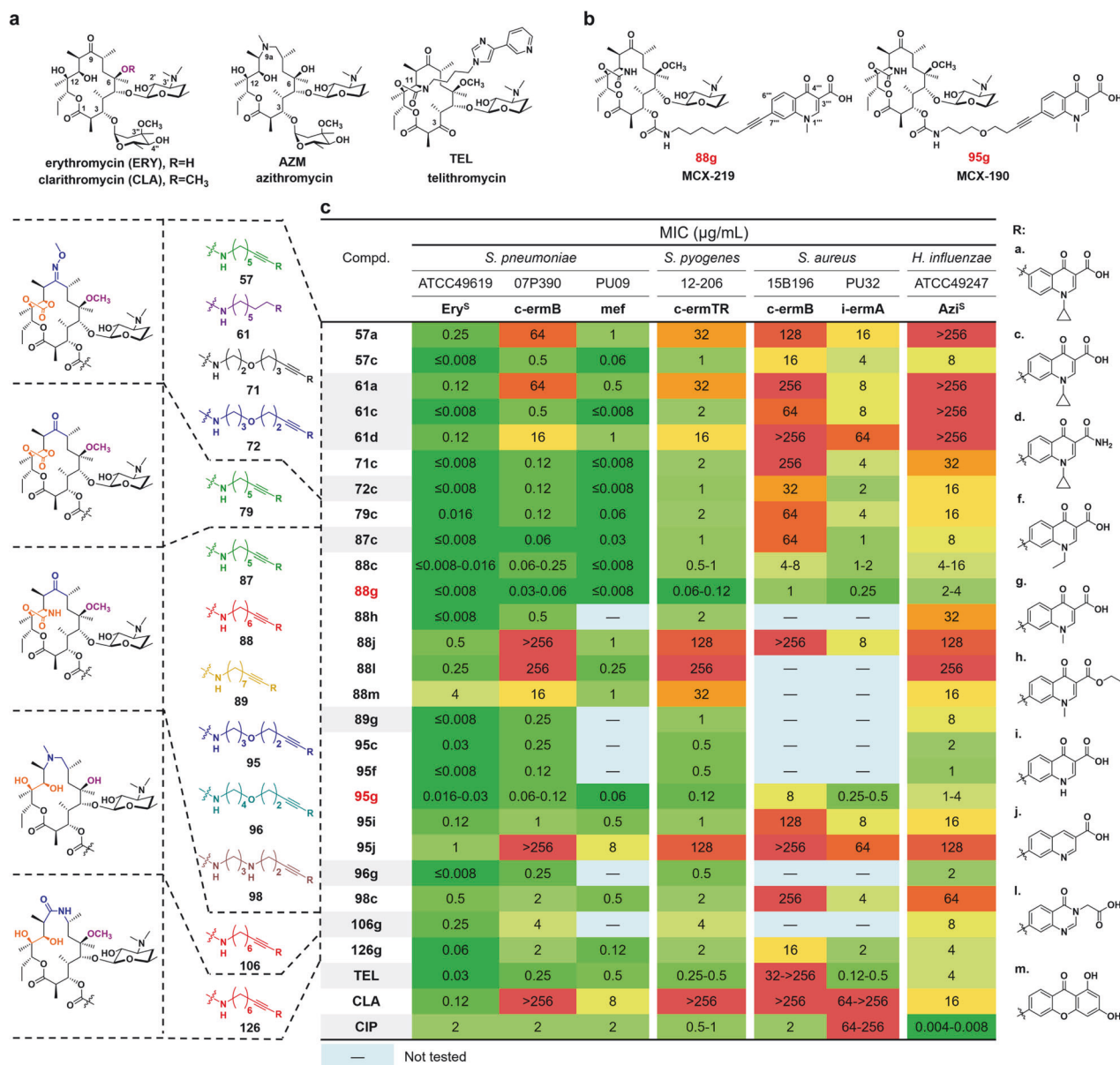


Fig. 1 The SARs of new hybrids of macrolides and quinolones. **a** Structures of the first-, second- and third-generation marketed erythromycins. **b** Structures of the representative macrolones MCX-219 and MCX-190. **c** MICs (μg/mL) of the selected synthetic macrolides. Ery^S erythromycin sensitive, AZM^S azithromycin sensitive, TEL telithromycin, CLA clarithromycin, CIP ciprofloxacin. The strains 07P390, PU09, 12-206, 15B196, and PU32 are erythromycin-resistant clinical isolates encoding various resistant genes.

the antibiotics of quinolones. Remarkably, 88g and 95g (coded MCX-219 and MCX-190, Fig. 1b) exhibited superior activities over telithromycin. We reasoned that the presence of an unsubstituted 1-NH in quinolones can lead to the formation of a tautomeric isomer known as 3-carboxy-4-hydroxyquinoline, which may be unfavorable for chelating function with a cation, such as Mg²⁺, as depicted in the mode of action of quinolones (95i vs 95g)⁴⁵.

A consistent trend was observed regarding the variation in linkers and quinolones on the 15-membered macrolide scaffold, for example, azithromycin, 8a-lactam, and 9a-lactam. Among them, 106g (azithromycin derivative) and 126g (8a-lactam derivative), both possessing the same linker and anchor as 88g (MCX-219), were the most potent, but less potent than the 14-membered MCX-219 and MCX-190. Detailed SARs are presented in Supplementary Fig. S1 and Tables S1–S8.

MCX-219 and MCX-190 overcome MLS_B resistance across pathogenic species

Strikingly, clinical isolates of *S. aureus*, irrespective of inducible or constitutive phenotypes, are susceptible to MCX-219 and MCX-190 (Fig. 2a). Furthermore, three mutant isolates of *M. pneumoniae* with mutations A2058G, A2059G, or A2058T are fully sensitive to MCX-219 and MCX-190. By contrast, telithromycin is inactive against both A2058-methylated *S. aureus* and A2058-mutated *M. pneumoniae*. Moreover, MCX-219 and MCX-190 demonstrate superior activity over telithromycin against clinical isolates of the other pathogens possessing various resistance types, such as *S. pneumoniae* and *S. pyogenes*, the majority of which might be the A2058-dimethylated as described by Douthwaite (Fig. 2a; Supplementary Table S9)²⁷.

Regardless of the categorization of the extensive clinical isolates of *S. aureus* (whether categorized into MRSA and

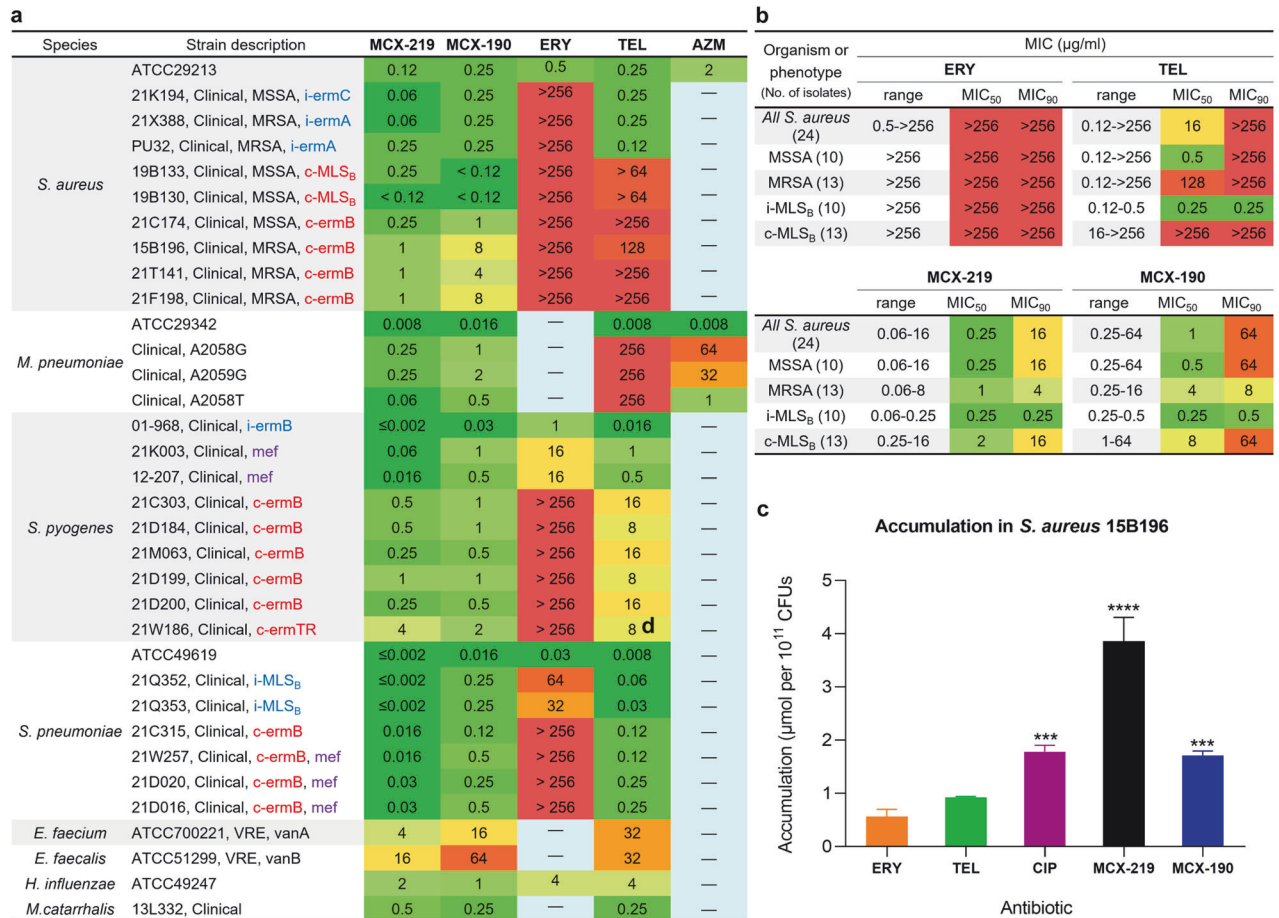


Fig. 2 MCX-219 and MCX-190 are active against a variety of resistant clinical isolates and highly accumulative inside cells. **a** MICs of MCX-219 and MCX-190 against *S. aureus*, *M. pneumoniae*, *S. pyogenes*, *S. pneumoniae*, *E. faecium*, *E. faecalis*, *H. influenzae* and *M. catarrhalis*. **b** MIC₅₀ and MIC₉₀ of erythromycin (ERY), telithromycin (TEL), MCX-219, and MCX-190 against 23 clinical isolates of *S. aureus* from hospitals in China, 2021. **c** Cellular accumulation in *S. aureus* 15B196 for MCX-219, MCX-190, ERY, TEL and ciprofloxacin (CIP). Data are expressed as mean ± SD and analyzed by using one-way ANOVA plus Dunnett. Statistical significance is reported as follows: **P* < 0.05, ***P* < 0.01, ****P* < 0.001, *****P* < 0.0001 vs ERY.

methicillin-susceptible *S. aureus* groups or alternatively into inducible and constitutive phenotype groups), notable reductions in MIC₅₀ values were observed for MCX-219 and MCX-190, rather than telithromycin, against the isolates collected in 2021 from various regions of China, known for their high resistance to antibiotics (Fig. 2b). For example, MCX-219 and MCX-190 had an MIC₅₀ of 1 μg/mL and 4 μg/mL against MRSA, respectively, while telithromycin had an MIC₅₀ of 128 μg/mL. Meanwhile, MCX-219 and MCX-190 had an MIC₅₀ of 2 μg/mL and 8 μg/mL against constitutive *S. aureus*, respectively, while telithromycin had an MIC₅₀ of > 256 μg/mL, further corroborating the activity of MCX series against constitutively erm-modified isolates.

The high accumulation inside cells is an important issue for designing new antibiotics⁴⁶. Unexpectedly, the enhanced activity of MCX-219 and MCX-190 against constitutively resistant *S. aureus* was partially contributed by their high cellular accumulation. It was found that MCX-219 and MCX-190 accumulated to a greater extent inside *S. aureus* cells with A2058-methylated ribosomes compared to telithromycin and erythromycin (Fig. 2c). MCX-219 accumulated twice as much as ciprofloxacin, although molecules with a considerably large molecular volume tend to exhibit low accumulation⁴⁶. Meanwhile, the higher accumulation of MCX-219 over MCX-190 accounted for higher in vivo inhibition of cell growth of MCX-219 over MCX-190, although MCX-219 and MCX-190 showed equal in vitro inhibition on the target (Refer to the following text).

MCX-219 showed bactericidal activity against 58.3% of *S. aureus* isolates (MBC/MIC ≤ 4), while telithromycin and its analog solithromycin (suspended in clinical phase III) were bacteriostatic against all selected isolates (Supplementary Fig. S2a and Table S10). Further study on time-kill kinetics also suggested that MCX-219 was bactericidal against constitutively erm-modified *S. aureus* 15B196, but bacteriostatic against inducibly erm-modified *S. aureus* PU32 (Supplementary Fig. S2b). In contrast to telithromycin, MCX-219 exhibited a decreased frequency of inducible resistance against susceptible *S. aureus* ATCC29213 and inducibly erm-modified *S. aureus* PU32 at a concentration of 4× MIC. Moreover, at concentrations of 8× MIC or 16× MIC, MCX-219 showed no inducible resistance against constitutively erm-modified *S. aureus* 15B196 that is insensitive to telithromycin (Supplementary Table S11).

Synthetic macrolides inhibit protein synthesis rather than DNA replication

The SARs of the synthetic hybrids, MCX-219 and MCX-190, have shown the essential role of the quinolone moiety in their antibacterial activity. Quinolone antibiotics target topoisomerase, a key enzyme involved in DNA supercoiling. DNA supercoiling is a crucial process in bacterial cells that involves the twisting and winding of the DNA double helix. Inhibition of DNA supercoiling can interfere with essential cellular functions, such as replication and transcription. While acknowledging the pivotal role of the

quinolone moiety in activities, we want to determine whether these hybrids are topoisomerase inhibitors or protein synthesis inhibitors.

An *in vivo* dual-reporter assay was conducted in engineered *E. coli* containing pDualrep2 reporter, in which the expression of Katushka2S protein (shown in red color) is induced in the presence of translation elongation inhibitors, while the expression of red fluorescent protein (RFP) (shown in green pseudo-color) is activated when exposed to compounds that cause DNA damage⁴⁷. Unlike ciprofloxacin, MCX-219 and MCX-190 displayed a red color inhibition zone, similar to the observation for erythromycin (Supplementary Fig. S3a).

In agreement with the results of the dual-reporter assay, these compounds showed *in vitro* minimal inhibition of *E. coli* DNA supercoiling, with IC₅₀ values greater than 100 μ M (Supplementary Fig. S3b). On the other hand, *in vitro* cell-free transcription/translation assays using materials from *E. coli* confirmed that MCX-219 and MCX-190 strongly inhibited protein synthesis with IC₅₀ values of 1.19 μ M and 0.67 μ M, respectively (Supplementary Fig. S3c).

To discern the mechanism by which macrolones impede bacterial growth, whether by targeting the ribosome or DNA gyrase, we opted to select and characterize spontaneous resistant mutants. SQ110DTC is an engineered *E. coli* strain with a sole chromosomal rRNA operon, designed specifically for researching ribosome-targeting antibiotics⁴⁸. When subjected to 3–9-fold MIC concentrations of MCX-219 and MCX-190, resistant colonies emerged. From these, twelve colonies (four for each concentration) were randomly chosen for sequencing to identify potential mutations in 23S rRNA and DNA gyrase. The resistance was found to stem from the mutations at A2058G or A2059G positions in the rRNA, with no mutations detected in the gyrase (Supplementary Fig. S4).

Collectively, the consistency in *in vitro* and *in vivo* assays suggests that the hybrids of macrolides and quinolones, exemplified by MCX-219 and MCX-190, exert their effects through function of protein synthesis inhibitors.

Structural basis for the SARs of the MCX series

The pronounced efficacy of MCX-190 against constitutively erm-modified *S. aureus* prompted us to investigate the structural basis for the SARs of our compounds, particularly focusing on how MCX-190 interacts with the ribosome at the molecular level.

We first purified 70S and 50S ribosomes from a wild-type (WT) *S. aureus* strain and a clinical isolate, MRSA 15B196. Notably, the 15B196 strain, constitutively erm-modified, demonstrates complete resistance to macrolides such as telithromycin, azithromycin, clarithromycin, and erythromycin.

We next determined the atomic structures of MCX-190 when bound to the 70S or 50S ribosomes from both strains using cryo-electron microscopy (Cryo-EM) (Supplementary Figs. S5–S7). Each of the four complexes revealed clear densities for MCX-190, localized within the NPET of the large ribosomal subunit (Fig. 3a, b). The absence of additional density for MCX-190 in the 30S subunit indicates that the NPET is the exclusive binding site for MCX-190. Structurally, the macrolactone ring of MCX-190 aligns similarly to other macrolides like erythromycin, with desosamine engaging with A2058 (*S. aureus* A2085). Remarkably, the quinolone moiety, extending ~8 angstroms away from the macrolactone ring, stacks atop the base pair C1782–C2586 (C1809–C2613) with its flat plane. It has been documented that A2062 (A2089) acts as a gatekeeper within NPET, selectively allowing certain nascent peptides with specific N termini to bypass and release them⁴⁹. The presence of the quinolone moiety causes a conformational shift of the gatekeeper A2062 (A2089), leading it to reposition next to the quinolone, unlike when ribosomes are bound to erythromycin or not bound to drugs (Supplementary Fig. S8). As a result, the quinolone becomes

sandwiched between the A2062 (A2089) and the C1782–C2586 (C1809–C2613) base pair (Fig. 3c).

The revelation of the quinolone binding site sheds light on the SARs of the MCX series of antibiotics. MCX-190, featuring a linkage at the C-7 position of the quinolone, retains potent activity, whereas alterations to the C-6 position, seen in compounds 57a and 61a, lead to a dramatic decrease in activity against constitutively erm-modified isolates. In the MCX-190–ribosome structure, the sandwiched quinolone is further stabilized by a water–magnesium bridge connecting the C3/C4 keto oxygen of the quinolone to the rRNA backbone phosphate of C2063, C2441, C2442, and C2586 (C2090, C2468, C2469, and C2613) (Fig. 3c). This stabilized interaction, contingent on the correct orientation of the quinolone, is ensured by the C-7 linkage (57c and 61c). This structural configuration is reminiscent of the one seen in the complex of ciprofloxacin with topoisomerase IV, where a similar water–magnesium bridge is crucial for the drug's activity⁴⁵. Such a bridge is potentially indispensable for MCX-190 targeting the ribosome. To further support this, 3-esterification (88h) or 3-amidation (61d) of the quinolone, known to significantly reduce the chelating ability of the carboxyl oxygen for metal ions, markedly deteriorates its activity.

Analysis of modifications at the N-1 position of the quinolone reveals that a methyl group confers the highest activity, while larger groups like ethyl and cyclopropyl result in a decrease in activity against constitutive *S. aureus*. Structurally, the quinolone of MCX-190 lies in the same plane as the adjacent base U2609 (U2636), with its methyl group oriented towards U2609 (U2636) at a distance of 4 angstroms. Our model suggests that bulkier chains, such as the ethyl group in compound 95f or a cyclopropyl group in 95c, could create steric clashes with U2609 (U2636), thus impeding activity (Fig. 3d). However, it would be intriguing to investigate the potential π – π interaction by incorporating a phenyl group, like the 2,4-difluorophenyl group, onto the N-1 position.

Finally, the linker connecting the quinolone and macrolactone ring plays a crucial role in determining the efficacy of the MCX series. The lead compounds, MCX-219 and MCX-190, though differing by one atom, share the same linker length. Variations resulting in either shorter (87c vs 88c) or longer linkers (88g vs 89g; 95g vs 96g) lead to decreased antibacterial efficacy. Structurally, in the MCX-190 complex, the linker adopts an L-shape, predominantly extended except at the turn. This conformation suggests a lack of structural tension, ensuring optimal alignment of the molecule. Furthermore, the linker packs against the C2610 (C2637) base, providing additional support for MCX-190 to bind to the ribosome (Fig. 3a). Our results suggest that the linker's spatial arrangement is critical in maximizing the compound's therapeutic potential.

MCX-190 targets WT and A2058-methylated ribosomes of *S. aureus*

To validate the *in vitro* activity of our compounds, we employed an *in vitro* reconstituted *E. coli* Protein synthesis Using a Recombinant Elements (PURE) translation system, substituting *E. coli* ribosomes with the purified *S. aureus* ribosomes. As depicted in Fig. 4a, erythromycin and telithromycin, along with MCX-219 and MCX-190, inhibited protein synthesis utilizing the WT *S. aureus* ribosomes. By contrast, the 15B196 ribosomes were sensitive to MCX-219 and MCX-190, mirroring the *in vivo* activity against erm-modified clinical isolates.

To assess the methylation status of A2058, we employed a modified method based on ref. ⁵⁰ and designed two distinct DNA probes to isolate rRNA fragments spanning 2052–2064 and 2055–2066 from both WT and 15B196 ribosomes. Quadrupole time-of-flight (TOF) mass spectrometry (QTOF-MS, Agilent 6545) was used to analyze the methylation at A2058. This technique allows for highly accurate mass measurements of RNA

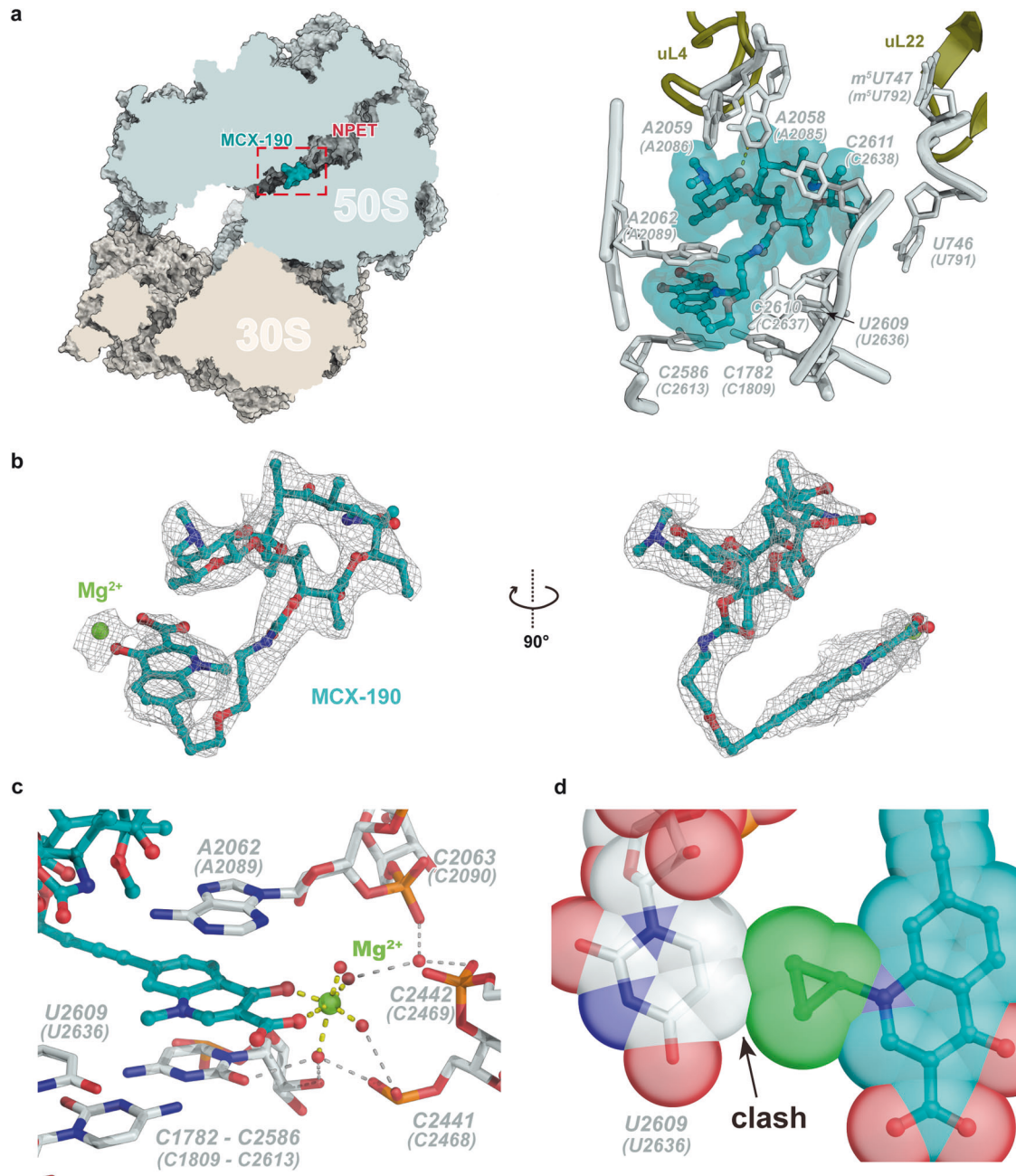


Fig. 3 Cryo-EM reconstruction of the complex of MCX-190 and WT ribosomes of *S. aureus*. **a** The overall and detail of MCX-190 bound to the NPET. The distance of the hydrogen bond between the 2'-OH of desosamine and N1 positions of A2058 (A2085) is 2.93 Å. **b** The density map of MCX-190 and cation Mg^{2+} in the WT ribosome complex. **c** Cation Mg^{2+} is chelated by the quinolone element and the other four H_2O molecules. **d** A cyclopropyl group at the N1 position of quinolone could create steric clashes with U2609 (U2636).

oligonucleotides, within 1.0 Da, facilitating the detection of mono-methylation (addition of 14 Da) and di-methylation (addition of 28 Da).

In the triply deprotonated ion, the nucleotide A2058 is present in the fragment GGACGGAAAGACC with a mass-to-charge ratio (m/z) of 1433.54 when unmethylated as seen for the WT ribosome. In the 15B196 ribosomes, additional masses corresponding to mono-methylation (1438.21 m/z) and di-methylation (1442.89 m/z) were observed (Fig. 4b). A similar pattern is observed in the fragment CGGAAAGACCCC (Supplementary Fig. S9). By integrating the peak areas (Supplementary Fig. S9), we determined the proportions of mono-methylation in the 15B196 ribosome to be

5.7% and 6.3%, and the proportions of di-methylation to be 40.4% and 37.3%, respectively. This suggests that the main modification is di-methylation.

The MCX-190–50S complexes were resolved at resolutions of 2.8 Å and 2.5 Å for the WT and 15B196 *S. aureus* ribosomes, respectively, which allowed us to verify base modifications (Supplementary Fig. S10). A2058 methylation is crucial for MLS_BK antibiotic resistance. When comparing the densities for A2058 in both 50S structures, we observed a peak emanating from the N6 of A2058 in the complex with the 15B196 ribosome (Fig. 4c), indicative of methylation. However, due to the low methylation level, the occupancy was expected to be low, which prevented us

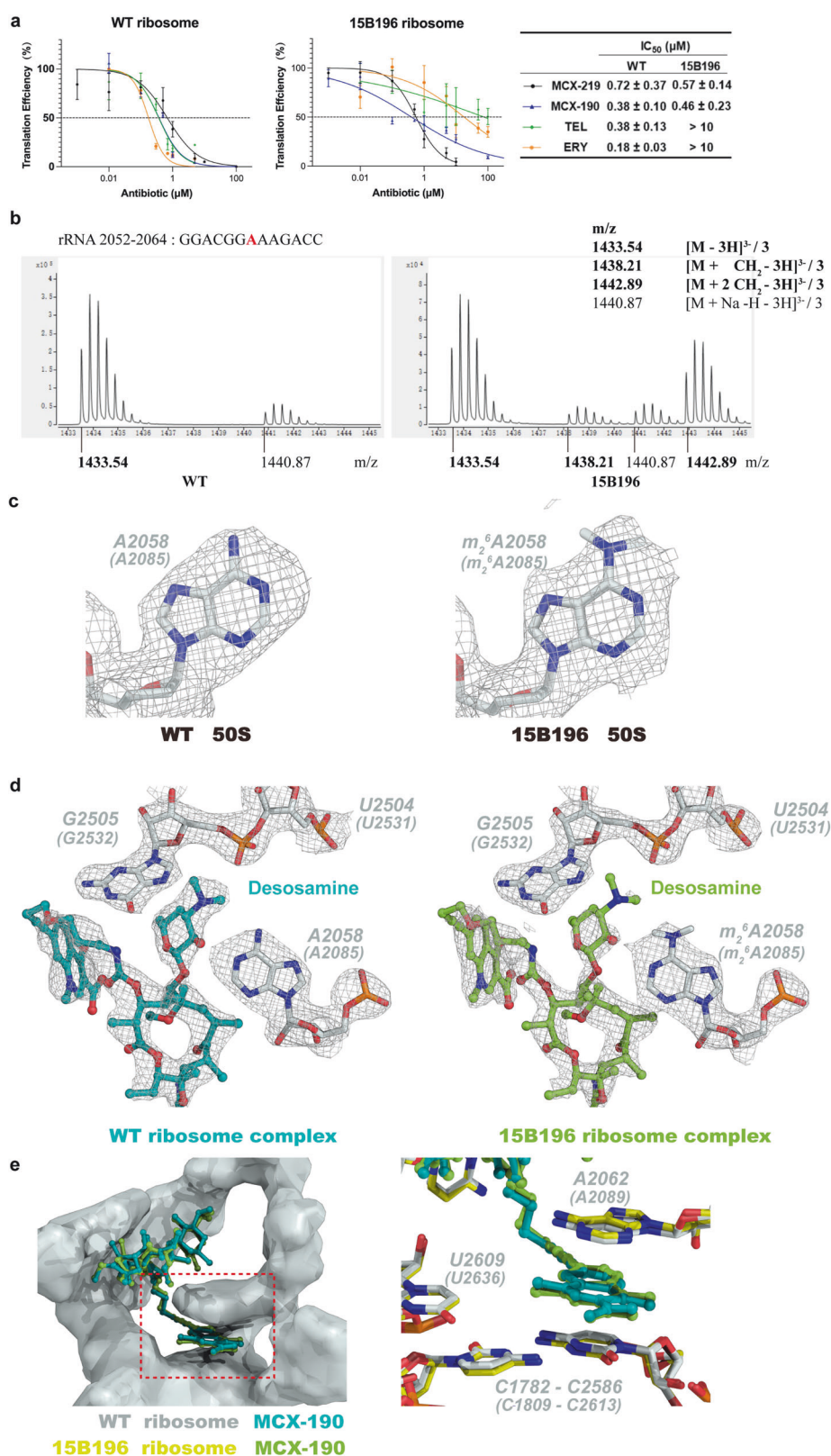


Fig. 4 Comparison of MCX-190 and WT/15B196 *S. aureus* ribosome complexes. **a** The results of in vitro translation inhibition assays showed that 15B196 ribosomes were sensitive to MCX-219 and MCX-190. IC₅₀ Values are shown as mean ± SD of at least three independent experiments. **b** Q-TOF mass spectrometry analysis of *S. aureus* rRNA 2052–2064. In the triply deprotonated ion of the molecule, the fragment GGACGGAAGACC runs at 1433.54 m/z (when unmethylated). Monomethylation and dimethylation at A2058 result in mass shifts to 1438.21 m/z and 1442.89 m/z, respectively. The unmethylated fragment with a Na ion is observed at 1440.87 m/z. **c** The density maps of A2058 (A2085) in the 15B196/WT *S. aureus* ribosome complex. Both of two density maps of are contoured at 7.5σ. **d** The density of the desosamine in the complex of 15B196 ribosome complex was significantly decreased, compared to the WT ribosome complex. **e** The π–π interaction of quinolone ring with A2062 (A2089) and C1782–C2586 (C1809–C2613), was not affected by whether A2058 (A2085) was methylated.

from clearly visualizing two methyl groups. Since the main modification is dimethylation, we modeled A2058 from the 15B196 ribosome as m₂⁶A2058. In both complexes, the desosamine of MCX-190 interacted with the unmodified A2058 and the methylated A2058 base via hydrogen bonding. Importantly, the interaction of the latter was weakened as confirmed by the decreased density of the desosamine in the complex of A2058-methylated ribosome (Fig. 4d).

Historically, methylation of A2058 has been known to weaken the interaction with the desosamine in macrolides, leading to high-level resistance^{1,7,8}. However, this weakened interaction can be compensated by introducing a secondary binding site. For instance, telithromycin, featuring a side-chain containing an aryl group that extends from the C-11 and C-12 positions, forms a stacking interaction with A752–U2609 (Supplementary Fig. S11)^{22–24}. This additional binding confers resistance to telithromycin against A2058-modified ribosomes. A similar rationale may elucidate the mechanism of MCX-190's activity: the quinolone ring establishes a new binding site, distanced from the mutation hotspot A2058 and thereby not affected by whether A2058 was methylated (Fig. 4e). Intriguingly, MCX-190 exhibits remarkable activity against *M. pneumoniae* clinical isolates harboring the A2058G mutation. Further investigations are warranted to elucidate how MCX-190 interacts with the A2058G-modified ribosome, potentially unveiling novel insights into its mode of action.

The rRNA base A2062, highly flexible, occludes the NPET lumen, and certain nascent peptides may cause it to reposition closer to the NPET wall, influencing peptide selective release^{49,51}. In the presence of erythromycin or telithromycin, there is still ample space for the nascent peptide chain to pass through the NPET (Supplementary Fig. S12). By contrast, when MCX-190 is bound, the NPET channel is completely obstructed due to the A2062 base flip and the presence of the quinolone side chain. Thus, the developed macrolone demonstrated a novel mechanism of action, which contributes to its remarkable effectiveness against various pathogenic species, including constitutively resistant *S. aureus* strains, which were previously unresponsive to existing MLS_BK treatments.

MCX-190 and MCX-219 do not inhibit human ribosome

We noted that a tetracyclic antibiotic, tetracenomycin X (TcmX) with a similar scaffold to doxorubicin and tetracycline, interacts U1782–U2586 base pair in the *E. coli* ribosome⁴⁷. Importantly, this report has verified that U1782–U2586, homologous C1782–C2586 in *S. aureus* and *S. pneumoniae*, is conserved across bacterial species. However, TcmX showed high cytotoxicity of ~2 μM and high inhibition on human ribosome at an IC₅₀ of 10 μM, limiting its further development in antibacterial application⁴⁷. Therefore, it is necessary to distinguish whether the cytotoxicity is caused by the structure of TcmX or its specific binding to the rRNA base pair C1782–C2586. The results from cytotoxicity assays in human HepG2 and HEK293T cells revealed that MCX-219 and MCX-190 demonstrated significantly reduced cytotoxicity compared to TcmX at a concentration of 5 μM (Fig. 5a). Furthermore, MCX-219 has a CC₅₀ of ~26–29 μM, while MCX-190 is essentially non-cytotoxic (Fig. 5b, c). Meanwhile, the inhibition of protein synthesis in human ribosomes treated by MCX-219 and MCX-190 is measured with IC₅₀ values of more than 100 μM (Fig. 5d). This comparison clearly indicated that the cytotoxicity of TcmX is basically related to its own structure.

CONCLUSION

The MLS_BK resistance associated with ribosomal alterations in clinical pathogens, particularly in relation to the primary target A2058, remains an unresolved problem. This has imposed

constraints on the development of MLS_BK antibiotics for an extended period. However, we have unveiled a novel and effective mode of action for the newly developed synthetic macrolides, such as their interaction with A2062 through a flipping mechanism and the subsequent sandwich-like A2062-quinolone-C1782/C2586 stacking mode of action within the NPET, the enhanced stabilization through a water–magnesium bridge. It is worth noting that currently available MLS_BK antibiotics including macrolones have shown an inability to effectively treat constitutively A2058-methylated *S. aureus*, attributed to species-specific effects. However, cryo-EM complex structures in this work have indicated that the methylation status of A2058 does not impact the contact between the quinolone element of MCX-190 and the new binding site, thereby firmly inhibiting protein synthesis of A2058-methylated ribosomes of *S. aureus*. This finding opens the possibility of utilizing quinolones as novel pharmacophores with unprecedented modes of action within ribosomes. Meanwhile, the optimal macrolides exhibited favorable drug-like properties, including low cytotoxicity to human cells, low induction of bacterial resistance, high cellular accumulation in cells, and high blood drug concentration in vivo (Supplementary Table S12).

In conclusion, the comprehensive SARs, combined with biological analysis and structural insights, illuminate the innovative modes of action of these optimized chemotypes. Our research provides a promising basis for the rational design of the next-generation MLS_BK to tackle prevalent resistance and expand the therapeutic reach to a broader spectrum of bacterial species.

MATERIALS AND METHODS

Susceptibility testing

MICs were determined by the microdilution method according to the Clinical and Laboratory Standards Institute guidelines. Briefly, the stock solution of compounds and the reference antibiotics were diluted 2-fold in sterile 96-well plates with cation-adjusted Mueller-Hinton broth, and mixed with CAMHB-containing bacteria to give a final inoculum of 5 × 10⁵ CFU/mL for broth microdilution experiments. The concentration range of the compounds typically employed for each experiment was 256–0.008 μg/mL (the final concentration of DMSO was kept below 1%). Finally, the 96-well plates were incubated at 37 °C for 16–20 h to observe and record the results. The lowest concentration at which no bacterial growth could be observed visually was identified as the MICs of the compounds. The assay for MICs was replicated at least three times.

Determination of antibacterial mechanism with pDualrep2 reporter

The reporter strain JW5503 Δ*toc* pDualrep2 has been utilized as described^{47,52}. We applied tested antibiotic solutions (spots of ciprofloxacin (1.65 ng), erythromycin (1.28 μg), MCX-190 (1.28 μg), and MCX-219 (6.4 μg)) to an agar plate that already contained a reporter strain lawn. The plate was incubated overnight at 37 °C, and then we scanned it with ChemoScope 6100 (Clinx, CN) using the 'Cy3-blot' mode for RFP and 'Cy5-blot' mode for Katushka2S. Katushka2S expression induction is triggered by translation inhibitors, whereas RFP up-regulation is a consequence of DNA damage and SOS response induction.

DNA supercoiling assay

The inhibition values of compounds on *E. coli* gyrase were determined using Gyrase Supercoiling Assay Kits purchased from Inspiralis (Norwich, UK). Supercoiling reaction mixtures, consisting of 35 mM Tris-HCl (pH 7.5), 24 mM KCl, 4 mM MgCl₂, 2 mM DTT, 1.8 mM Spermidine, 1 mM ATP, 6.5% (w/v) glycerol, 0.1 mg/mL BSA, 1 U of DNA gyrase, 0.5 μg of relaxed pBR322 DNA and various concentrations of compounds (ciprofloxacin, MCX-219, MCX-190, 106g, 126g) were incubated at 37 °C for 30 min. Ciprofloxacin was employed as a gyrase inhibitor control. The addition of 30 μL Stop Buffer and 30 μL chloroform/iso-amyl alcohol (24/1) stopped each reaction. The DNA products were analyzed by electrophoresis through 1% agarose gels in TAE buffer. After being stained with 0.5 μg/mL ethidium bromide, the gels were photographed and quantified using ChemoScope 6100 (Clinx, China).

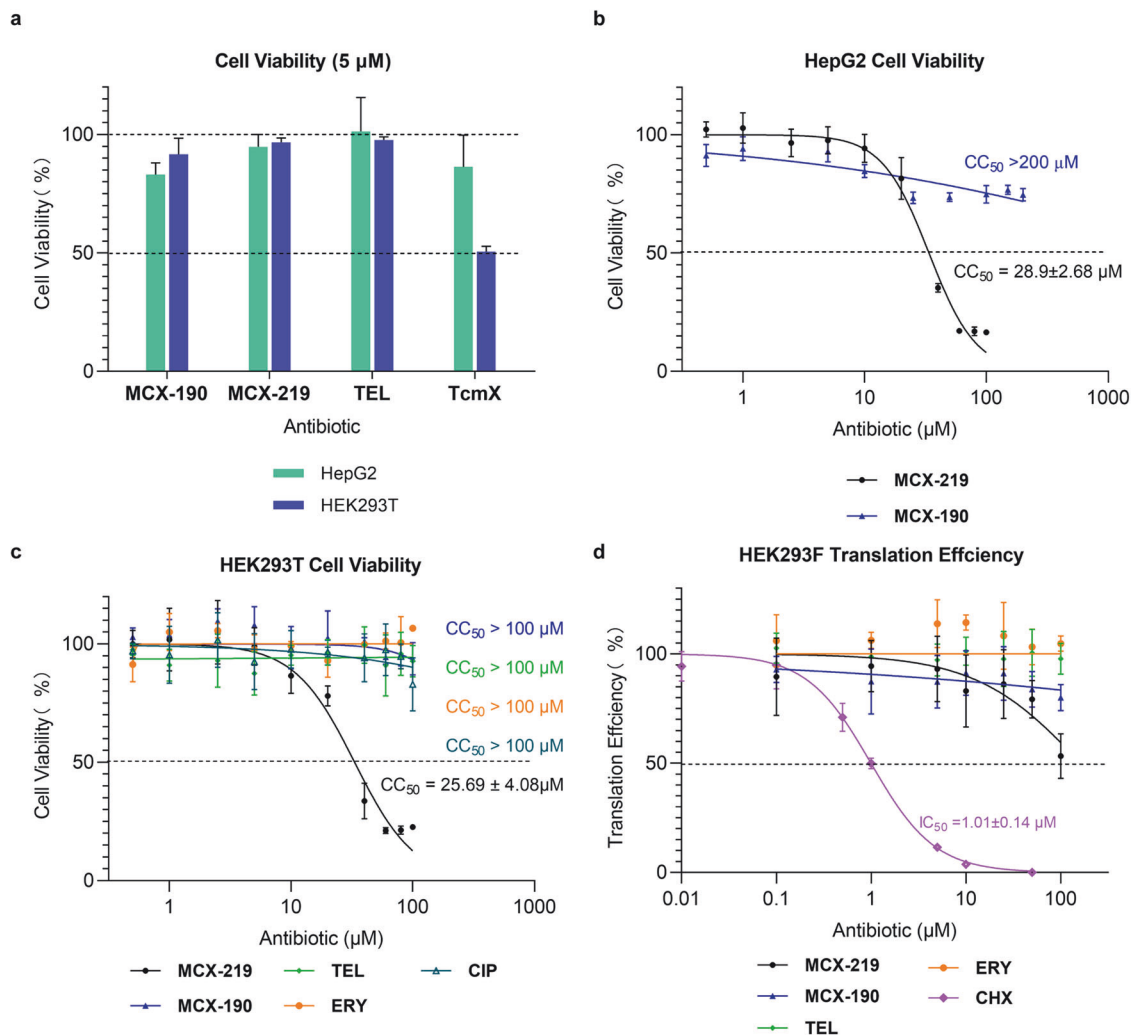


Fig. 5 Cytotoxicity and inhibition of eukaryotic translation by MCX-219 and MCX-190. **a** Cytotoxicity of the optimal compounds at a concentration of 5 μ M with an incubation for 48 h. **b**, **c** Cell viability of HepG2 (**b**) and HEK293T (**c**) cells in the presence of increasing concentrations of MCX-219 or MCX-190. MCX-219 showed a calculated cytotoxicity concentration at 26 μ M that inhibits 50% viability (CC_{50}), while TcmX reportedly had a CC_{50} of 2 μ M (**c**). **d** In vitro translation of Fluc mRNA in HEK293F whole-cell lysate in increasing concentrations of MCX-219 or MCX-190. CHX cycloheximide. Values are shown as the mean \pm SD of at least three independent experiments.

Time-kill kinetics assay

To further determine the bactericidal activity of MCX-219, a time-kill assay was performed according to the method described previously⁵³. The *S. aureus* cultured overnight was diluted 10^4 times with CAMHB broth and incubated for 2 h. Different concentrations of compounds (1 \times MIC, 2 \times MIC, 4 \times MIC, 8 \times MIC) were added to the bacterial broth and placed in a shaker to continue the incubation for 24 h. The number of colonies was measured at 0 h, 1 h, 3 h, 6 h, 9 h and 24 h. A flask containing bacteria left unexposed to antibiotic was used as blank control, and telithromycin was used as the positive drug (comparator drug).

Frequency of resistance

Luria-Bertani (LB) agar plates containing the compound at concentrations corresponding to 4 \times MIC, 8 \times MIC, and 16 \times MIC were prepared. Bacterial cultures of *S. aureus* strains ATCC 29213, PU32, and 15B196 were generated through overnight cultivation, and bacterial counts were determined by serial dilution and plating. 200 μ L of bacterial inocula (containing $\sim 1 \times 10^7$, 1×10^8 , and 1×10^9 CFU, respectively) were evenly spread over the media plates. The plates were then incubated at 37 $^{\circ}$ C for 72 h, and the appearance of the colony was regularly monitored throughout this period.

Accumulation assay

Assays were conducted according to previous reports⁴⁶. In these experiments, the strain *S. aureus* 15B196 was employed. 1 mL of an

overnight culture of *S. aureus* 15B196 was diluted in 100 mL of fresh LB broth and grown at 37 $^{\circ}$ C with shaking to an optical density (OD_{600}) of 0.55. After incubation, the cells were centrifuged to separate them from the supernatant, which was subsequently removed. Subsequently, the cells were washed once with 30 mL of phosphate-buffered saline before being resuspended. Each experimental tube was then filled with 200 μ L of bacterial suspension and incubated with shaking for 5 min. Finally, the antibiotic (MCX-219, MCX-190, erythromycin, telithromycin, or ciprofloxacin) was added to reach a concentration of 50 μ M, and the incubation was continued for an additional 10 min. Prior to initiating the experiment, tubes were prepared by adding 300 μ L of silicone oil (9:1 AR20/Sigma high temperature, cooled to -78° C). A 200 μ L layer of bacterial suspension was carefully added over the silicone oil cushion in each tube, ensuring that the oil layer was completely thawed before subjecting the tubes to centrifugation at 13,000 \times g for 2 min at room temperature. Finally, both the supernatant and oil were thoroughly removed. The resulting pellets of *S. aureus* were resuspended in a 20 μ L of buffer containing 2 mg/mL of lysostaphin. The suspension was then incubated at 37 $^{\circ}$ C for 30 min. After the incubation, 30 μ L of H₂O was added before freezing the mixture in liquid nitrogen. Three cycles of freezing/thawing were performed, with each cycle lasting 3 min in liquid nitrogen, followed by incubation in a water bath at 65 $^{\circ}$ C for 3 min. Subsequently, the tubes were centrifuged at 13,000 \times g for 2 min at room temperature, and the precipitate was washed with 100 μ L of methanol. The mixture of supernatant was analyzed using Liquid Chromatography-Mass Spectrometry/Mass Spectrometry

(LC-MS/MS). The quantification of drug concentration in the samples was quantified using the external standard method.

In vitro *E. coli* transcription/translation assay

The in vitro transcription/translation assay for *E. coli* utilized materials from the *E. coli* S30 extract system for circular DNA (L1020, Promega, USA). This kit contains all the necessary components for efficient transcription and translation of a user-provided DNA template. To test the inhibition of protein synthesis, the assay uses plasmid pBESTluc, which contains the firefly luciferase gene, as the DNA template. The intensity of luminescence resulting from luciferase expression corresponds to the efficiency of protein synthesis. The luminescence intensity was quantified in the presence or absence of the tested compounds. The compounds were evaluated at concentrations of 5 μ M, 1 μ M, 0.5 μ M, 0.1 μ M, and 0.01 μ M to determine IC₅₀ values. This experiment was repeated twice independently.

Selection of resistant mutants in SQ110DTC

The *E. coli* strain SQ110DTC, which carries a single *rme* allele and Δ tolC mutation, was cultured overnight in LB medium supplemented with kanamycin (50 μ g/mL). Subsequently, the cells were plated on LB agar plates containing kanamycin (50 μ g/mL) along with various concentrations of the compounds, specifically around 3 \times , 6 \times or 9 \times MIC. After incubation at 37 °C for 48 h, ~20 colonies were observed on plates. 23S rRNA gene was then amplified using PCR and sequenced using the primers as previously described⁴⁸. The *GyrA* gene was amplified using the primers GCGATGTCGGTCATTGTT and ACTTCCGGTCAGGTGTGTC.

Animal studies

All experimental processes were conducted in strict compliance with the experimental animal management regulations and animal ethics policies of Beijing Institute of Technology. Pathogen-free male SD rats weighing 200 \times g were obtained from Peking University Health Science Center. Animals were acclimatized for at least 3 days before the start of the studies and were exposed to a 12-h light/dark cycle. Animals were kept under controlled conditions with food and water ad libitum.

In vivo pharmacokinetic study

The SD rats were fasted overnight and dosed i.v. at a dose of 5 mg/kg in a solution of DMSO/PEG 400/water (5%/24%/71%). The whole blood was collected into tubes containing sodium heparin at 0.083 h, 0.25 h, 0.5 h, 1 h, 2 h, 4 h, 8 h and 24 h after dosing. After centrifugation of 6000 rpm for 10 min at 4 °C, plasma samples were transferred into 1.5 mL tubes and stored at -20 °C. Prior to analysis, the samples were thawed on ice. An amount of 50 μ L of each plasma sample was added to a mixture of 50 μ L of propranolol (300 ng/mL) and 100 μ L of acetonitrile and centrifuged at 12,000 rpm at 4 °C for 10 min. The supernatant was diluted and analyzed by LC-MS/MS. The liquid chromatography was conducted on a Thermo Scientific Q Exactive HF-X (ThermoFisher Scientific, USA) instrument, employing an ACQUITY UPLC BEH C18 Column with dimensions of 130 Å, 1.7 μ m, 2.1 mm \times 100 mm. The liquid phase method employed gradient elution with mobile phases consisting of acetonitrile and an 0.1% aqueous formic acid solution. Mass spectrometry was conducted in positive ion mode. The quantification of drug concentration in plasma samples was performed using the internal standard method, and the obtained pharmacokinetic parameters were calculated using Phoenix WinNonlin software.

Cell culture

HEK293T (3101HUMGNHu17) and HepG2 (1101HUM-PUMC000035) cell lines were obtained from the Cell Resource Center, Peking Union Medical College. All were acquired in 2023 and were maintained in culture for no more than 30 continuous passages. The cells were cultured in DMEM (11995065, Gibco) supplemented with 10% FBS (164210-50, Procell), 100 units penicillin and 100 mg/mL streptomycin (PB180120, Procell).

CCK-8 assay for cytotoxicity

HepG2 cells (6 \times 10³) and HEK293T cells (4 \times 10³) were seeded into 96-well plates in 90 μ L of DMEM medium containing 10% FBS per well. All test compounds were formulated as 10 mM stock solutions in DMSO (final concentration \leq 0.5%). After overnight incubation, the test compound stock solution was diluted with DMEM medium containing 10% FBS to every target concentration, and 10 μ L of each was added to each well.

Three parallel experiments were set up for each compound. After incubation for 48 h, 10 μ L of cell counting kit-8 (CCK-8) reagent was added to each well in sequence according to the manufacturer's instructions. After incubating in a 37 °C incubator for 1–2 h, the absorbance was measured at a wavelength of 450 nm, and detected by ThermoScientific Multiskan FC (ThermoFisher Scientific, USA). This experiment was independently repeated three times. The data were processed by GraphPad Prism.

Ribosome purification

Ribosomes were purified from *S. aureus* WT/15B196 as previously described⁵⁴, with minor modifications. The cells were lysed in buffer A (20 mM HEPES-KOH pH 7.5, 100 mM NH₄Cl, 10.5 mM Mg-acetate, 0.5 mM EDTA-Na pH 8.0, 4 mM DTT, 150 mM sucrose) and the lysate was clarified by centrifugation. Following ultracentrifugation for 20 h (43,000 rpm) at 4 °C in the Type 45Ti rotor (Beckman Coulter, USA), the ribosome pellets were resuspended in the buffer B (10 mM HEPES-KOH pH 7.5, 50 mM KCl, 10 mM NH₄Cl, 1.25 mM Mg-acetate, 0.25 mM EDTA-Na pH 8.0, 4 mM DTT). Subsequently, the ribosomes were separated by centrifugation through 15%–40% sucrose gradients in the SW32 rotor at 28,000 rpm for 16 h. 50S and 30S ribosomes were separated by ÄKTA pure™ chromatography system (Cytiva), and buffer exchanged into 5 mM HEPES-KOH pH 7.5, 60 mM NH₄Cl, 10 mM MgCl₂, 4 mM DTT, flash-frozen in liquid nitrogen and stored at -80 °C.

Sample preparation

MCX-190-WT ribosome complexes were prepared by incubating 0.2 μ M 30S, 0.3 μ M 50S in 1 \times ribosome buffer (20 mM Tris-HCl pH 7.5, 100 mM KCl, 10 mM MgCl₂, 2 mM DTT) at 37 °C for 10 min. Then MCX-190 to a final concentration of 5 μ M was added and incubated for another 10 min. Finally, the complexes were transferred on ice for cryo-grid preparation. MCX-190–15B196 ribosome complexes were prepared using the same procedure.

Cryo-grid preparation, data collection, and processing

To prepare cryo-EM grids, 2.5 μ L of the sample was applied onto the R1.2/1.3 300 mesh holey carbon Au grids with graphene oxide (Quantifoil) and left absorption for 8 s in the chamber under 100% humidity at 4 °C. The grids were blotted for 2–4 s in a VitroBot Mark IV (ThermoFisher Scientific, USA) and plunge-frozen in liquid ethane at liquid nitrogen temperature. The ϕ 55/20 mm blotting paper was used for plunge freezing (TED PELLA).

All the cryo-EM images were automatically recorded on a Titan Krios (ThermoFisher Scientific) transmission electron microscope by a post-GIF Gatan K3 direct electron detector in the super-resolution mode using EPU software (version 2.8.2.10REL) with a nominal magnification of 81,000 \times in the ETTEM mode, which yielded a super-resolution pixel size of 0.412 Å on the image plane, and with a defocus ranged from 0.5 to 1.5 μ m. Each micrograph stack was dose-fractionated into 40 frames with a total electron dose of \sim 50 e⁻/Å². 10,537 micrographs out of 11,326 movies for wide type-ribosome and 11,959 micrographs out of 12,426 movies for 15B196-ribosome were selected for further processing.

For cryo-EM data processing, drift and beam-induced motion correction were applied on the super-resolution movie stacks using MotionCor2⁵⁵ and binned 2-fold to a calibrated pixel size of 0.824 Å/pix. The defocus values were estimated by CTFFIND4⁵⁶ from summed images without dose weighting. As for 15B196-ribosome data, an initial set of 1,762,848 particles was used for 2D classification in RELION⁵⁷. 1,644,372 particles were selected from useful 2D classes for the initial 3D classification, using a 60 Å low-pass filtered ab-initial model reconstructed in cryoSPARC⁵⁸. For the 50S-complex, 68,392 particles were selected and refined to 2.53 Å resolution by NU-refinement⁵⁹. For the 70S-complex, 47,560 particles were used and reconstituted to 2.58 Å resolution. To refine the MCX-190 structure, a masked local refinement followed by a masked local 3D classification focused on the NPET in RELION. As for WT ribosome data, an initial set of 1,207,936 particles was used for 2D classification in RELION⁵⁷. 976,215 particles were selected from useful 2D classes for the initial 3D classification, using a 60 Å low-pass filtered ab-initial model reconstructed in cryoSPARC⁵⁸. For the 50S-complex, 666,754 particles were selected and refined to 2.65 Å resolution by NU-refinement⁵⁹. For the 70S-complex, 27,177 particles were used and reconstituted to 3.60 Å resolution. To refine the MCX-190 structure, a masked local refinement followed by a masked local 3D classification focused on the NPET in RELION.



5. Flamm, R. K., Rhomberg, P. R. & Sader, H. S. In vitro activity of the novel lactone ketolide nafthromycin (WCK 4873) against contemporary clinical bacteria from a global surveillance program. *Antimicrob. Agents Chemother.* **61**, e01230 (2017).
6. Farrell, D. J., Flamm, R. K., Sader, H. S. & Jones, R. N. Results from the solithromycin international surveillance program (2014). *Antimicrob. Agents Chemother.* **60**, 3662–3668 (2016).
7. Svetlov, M. S. et al. Structure of Erm-modified 70S ribosome reveals the mechanism of macrolide resistance. *Nat. Chem. Biol.* **17**, 412–420 (2021).
8. Lin, J. Z., Zhou, D. J., Steitz, T. A., Polikanov, Y. S. & Gagnon, M. G. Ribosome-targeting antibiotics: modes of action, mechanisms of resistance, and implications for drug design. *Annu. Rev. Biochem.* **87**, 451–478 (2018).
9. Miklasinska-Majdanik, M. Mechanisms of resistance to macrolide antibiotics against *Staphylococcus aureus*. *Antibiotics* **10**, 1406 (2021).
10. Kaneko, T., Dougherty, T. J. & Magee, T. V. 7.18 — Macrolide antibiotics. In *Comprehensive Medicinal Chemistry II*, Vol. 7 (eds Taylor, J. B., & Triggler D. J.) 519–566 (Elsevier Press, 2007).
11. Pavlovic, D., Fajdetic, A. & Mutak, S. Novel hybrids of 15-membered 8a- and 9a-azahomoerythromycin A ketolides and quinolones as potent antibacterials. *Bioorg. Med. Chem.* **18**, 8566–8582 (2010).
12. Seiple, I. B. et al. A platform for the discovery of new macrolide antibiotics. *Nature* **533**, 338–345 (2016).
13. Mitchelltree, M. J. et al. A synthetic antibiotic class overcoming bacterial multidrug resistance. *Nature* **599**, 507–512 (2021).
14. Wu, K. J. Y. et al. An antibiotic preorganizing for ribosomal binding overcomes antimicrobial resistance. *Science* **383**, 721–726 (2024).
15. Pereyre, S., Goret, J. & Bebear, C. *Mycoplasma pneumoniae*: current knowledge on macrolide resistance and treatment. *Front. Microbiol.* **7**, 974 (2016).
16. Svetlov, M. S. et al. Context-specific action of macrolide antibiotics on the eukaryotic ribosome. *Nat. Commun.* **12**, 2803 (2021).
17. Agouridas, C. et al. Synthesis and antibacterial activity of ketolides (6-O-methyl-3-oxoerythromycin derivatives): A new class of antibacterials highly potent against macrolide-resistant and -susceptible respiratory pathogens. *J. Med. Chem.* **41**, 4080–4100 (1998).
18. Tanikawa, T. et al. Synthesis and antibacterial activity of acylides (3-O-acyl-erythromycin derivatives): A novel class of macrolide antibiotics. *J. Med. Chem.* **44**, 4027–4030 (2001).
19. Tang, D. et al. Design, synthesis, and antibacterial activities of novel 3,6-bicyclic oximes: Length optimization and zero carbon linker oximes. *Bioorg. Med. Chem. Lett.* **18**, 5078–5082 (2008).
20. Liang, J.-H. et al. Structure-activity relationships of novel alkylides: 3-O-Arylalkyl clarithromycin derivatives with improved antibacterial activities. *Eur. J. Med. Chem.* **49**, 289–303 (2012).
21. Magee, T. V. et al. Novel 3-O-carbamoyl erythromycin A derivatives (carbamolides) with activity against resistant staphylococcal and streptococcal isolates. *Bioorg. Med. Chem. Lett.* **23**, 1727–1731 (2013).
22. Dunkle, J. A., Xiong, L., Mankin, A. S. & Cate, J. H. D. Structures of the *Escherichia coli* ribosome with antibiotics bound near the peptidyl transferase center explain spectra of drug action. *Proc. Natl. Acad. Sci. USA* **107**, 17152–17157 (2010).
23. Bulkley, D., Innis, C. A., Blaha, G. & Steitz, T. A. Revisiting the structures of several antibiotics bound to the bacterial ribosome. *Proc. Natl. Acad. Sci. USA* **107**, 17158–17163 (2010).
24. Llano-Sotelo, B. et al. Binding and action of CEM-101, a new fluoroketolide antibiotic that inhibits protein synthesis. *Antimicrob. Agents Chemother.* **54**, 4961–4970 (2010).
25. Eyal, Z. et al. Structural insights into species-specific features of the ribosome from the pathogen *Staphylococcus aureus*. *Proc. Natl. Acad. Sci. USA* **112**, E5805–E5814 (2015).
26. Georgopapadakou, N. H. The wobbly status of ketolides: where do we stand? *Expert Opin. Investig. Drugs* **23**, 1313–1319 (2014).
27. Douthwaite, S., Jalava, J. & Jakobsen, L. Ketolide resistance in *Streptococcus pyogenes* correlates with the degree of rRNA dimethylation by Erm. *Mol. Microbiol.* **58**, 613–622 (2005).
28. Paljetak, H. C. et al. Macrolones are a novel class of macrolide antibiotics active against key resistant respiratory pathogens in vitro and in vivo. *Antimicrob. Agents Chemother.* **60**, 5337–5348 (2016).
29. Paljetak, H. C. et al. Macrolide hybrid compounds: drug discovery opportunities in anti-infective and anti-inflammatory area. *Curr. Top. Med. Chem.* **17**, 919–940 (2017).
30. Domalaon, R., Idowu, T., Zhanel, G. G. & Schweizer, F. Antibiotic hybrids: the next generation of agents and adjuvants against gram-negative pathogens? *Clin. Microbiol. Rev.* **31**, e00077–17 (2018).
31. Hutinec, A. et al. Novel 8a-aza-8a-homoerythromycin-4''-(3-substituted-amino) propionates with broad spectrum antibacterial activity. *Bioorg. Med. Chem. Lett.* **20**, 3244–3249 (2010).
32. Skugor, M. M. et al. Synthesis and biological activity of 4''-O-acyl derivatives of 14- and 15-membered macrolides linked to omega-quinolone-carboxylic unit. *Bioorg. Med. Chem.* **18**, 6547–6558 (2010).
33. Kapic, S. et al. 6-Alkylquinolone-3-carboxylic acid tethered to macrolides synthesis and antimicrobial profile. *Bioorg. Med. Chem.* **18**, 6569–6577 (2010).
34. Fajdetic, A. et al. 4''-O-(omega-Quinolylamino-alkylamino)propionyl derivatives of selected macrolides with the activity against the key erythromycin resistant respiratory pathogens. *Bioorg. Med. Chem.* **18**, 6559–6568 (2010).
35. Jakopovic, I. P. et al. Synthesis and properties of macrolones characterized by two ether bonds in the linker. *Bioorg. Med. Chem.* **18**, 6578–6588 (2010).
36. Fajdetic, A. et al. Synthesis, activity and pharmacokinetics of novel antibacterial 15-membered ring macrolones. *Eur. J. Med. Chem.* **46**, 3388–3397 (2011).
37. Kapic, S. et al. Synthesis and activity of new macrolones: conjugates between 6''-(2'-aminoethyl)-amino-1-cyclopropyl-3-carboxylic acid (2'-hydroxyethyl) amides and 4-propenyl-azithromycin. *Bioorg. Med. Chem.* **19**, 7270–7280 (2011).
38. Kapic, S. et al. Synthesis of macrolones with central piperazine ring in the linker and its influence on antibacterial activity. *Bioorg. Med. Chem.* **19**, 7281–7298 (2011).
39. Pavlovic, D. & Mutak, S. Discovery of 4''-ether linked azithromycin-quinolone hybrid series: influence of the central linker on the antibacterial activity. *ACS Med. Chem. Lett.* **2**, 331–336 (2011).
40. Pavlovic, D. & Mutak, S. Synthesis and antibacterial evaluation of novel 4''-glycyl linked quinolyl-azithromycins with potent activity against macrolideresistant pathogens. *Bioorg. Med. Chem.* **24**, 1255–1267 (2016).
41. Pavlovic, D., Kimmins, S. & Mutak, S. Synthesis of novel 15-membered 8a-azahomoerythromycin A acylides: Consequences of structural modification at the C-3 and C-6 position on antibacterial activity. *Eur. J. Med. Chem.* **125**, 210–224 (2017).
42. Ma, C. X. et al. Design, synthesis and structure-activity relationships of novel macrolones: hybrids of 2-fluoro 9-oxime ketolides and carbamoyl quinolones with highly improved activity against resistant pathogens. *Eur. J. Med. Chem.* **169**, 1–20 (2019).
43. Fan, B.-Z. et al. Design, synthesis and structure-activity relationships of novel 15-membered macrolides: quinolone/quinoline-containing sidechains tethered to the C-6 position of azithromycin acylides. *Eur. J. Med. Chem.* **193**, 112222 (2020).
44. Liu, X. P. et al. Design and synthesis of novel macrolones bridged with linkers from 11,12-positions of macrolides. *Bioorg. Med. Chem. Lett.* **68**, 128761 (2022).
45. Aldred, K. J., Kerns, R. J. & Osheroff, N. Mechanism of quinolone action and resistance. *Biochemistry* **53**, 1565–1574 (2014).
46. Richter, M. F. et al. Predictive compound accumulation rules yield a broad-spectrum antibiotic. *Nature* **545**, 299–304 (2017).
47. Osterman, I. A. et al. Tetracenomycin X inhibits translation by binding within the ribosomal exit tunnel. *Nat. Chem. Biol.* **16**, 1071–1080 (2020).
48. Orelle, C. et al. Tools for characterizing bacterial protein synthesis inhibitors. *Antimicrob. Agents Chemother.* **57**, 5994–6004 (2013).
49. Kannan, K., Vazquez-Laslop, N. & Mankin, A. S. Selective protein synthesis by ribosomes with a drug-obstructed exit tunnel. *Cell* **151**, 508–520 (2012).
50. Andersen, T. E., Porse, B. T. & Kirpekar, F. A novel partial modification at C2501 in *Escherichia coli* 23S ribosomal RNA. *RNA* **10**, 907–913 (2004).
51. Zhang, W. et al. Cryo-EM structure of *Mycobacterium tuberculosis* 50S ribosomal subunit bound with clarithromycin reveals dynamic and specific interactions with macrolides. *Emerg. Microbes Infect.* **11**, 293–305 (2022).
52. Osterman, I. A. et al. Sorting out antibiotics' mechanisms of action: a double fluorescent protein reporter for high-throughput screening of ribosome and DNA biosynthesis inhibitors. *Antimicrob. Agents Chemother.* **60**, 7481–7489 (2016).
53. Kong, H. T. et al. Development of aromatic-linked diamino acid antimicrobial peptide mimics with low hemolytic toxicity and excellent activity against methicillin-resistant *Staphylococcus aureus* (MRSA). *J. Med. Chem.* **66**, 7756–7771 (2023).
54. Zhou, D., Tanzawa, T., Lin, J. & Gagnon, M. G. Structural basis for ribosome recycling by RRF and tRNA. *Nat. Struct. Mol. Biol.* **27**, 25–32 (2020).
55. Zheng, S. Q. et al. MotionCor2: anisotropic correction of beam-induced motion for improved cryo-electron microscopy. *Nat. Methods* **14**, 331–332 (2017).
56. Rohou, A. & Grigorieff, N. CTFFIND4: fast and accurate defocus estimation from electron micrographs. *J. Struct. Biol.* **192**, 216–221 (2015).
57. Zivanov, J. et al. New tools for automated high-resolution cryo-EM structure determination in RELION-3. *Elife* **7**, e42166 (2018).
58. Punjani, A., Rubinstein, J. L., Fleet, D. J. & Brubaker, M. A. cryoSPARC: algorithms for rapid unsupervised cryo-EM structure determination. *Nat. Methods* **14**, 290–296 (2017).
59. Punjani, A., Zhang, H. & Fleet, D. J. Non-uniform refinement: adaptive regularization improves single-particle cryo-EM reconstruction. *Nat. Methods* **17**, 1214–1221 (2020).
60. Williams, C. J. et al. MolProbity: more and better reference data for improved all-atom structure validation. *Protein Sci.* **27**, 293–315 (2017).
61. Pettersen, E. F. et al. UCSF Chimera — a visualization system for exploratory research and analysis. *J. Comput. Chem.* **25**, 1605–1612 (2004).

62. Pettersen, E. F. et al. UCSF ChimeraX: structure visualization for researchers, educators, and developers. *Protein Sci.* **30**, 70–82 (2020).
63. Grossman, T. H. et al. Target- and resistance-based mechanistic studies with TP-434, a novel fluorocycline antibiotic. *Antimicrob. Agents Chemother.* **56**, 2559–2564 (2012).
64. Jenner, L. et al. Structural basis for potent inhibitory activity of the antibiotic tigecycline during protein synthesis. *Proc. Natl. Acad. Sci. USA.* **110**, 3812–3816 (2013).
65. Terenin, I. M., Andreev, D. E., Dmitriev, S. E. & Shatsky, I. N. A novel mechanism of eukaryotic translation initiation that is neither m7G-cap-, nor IRES-dependent. *Nucleic Acids Res.* **41**, 1807–1816 (2013).
66. Prokhorova, I. V. et al. Amicoumacin A induces cancer cell death by targeting the eukaryotic ribosome. *Sci. Rep.* **6**, 27720 (2016).
67. Akulich, K. A. et al. Four translation initiation pathways employed by the leaderless mRNA in eukaryotes. *Sci. Rep.* **6**, 37905 (2016).



Open Access This article is licensed under a Creative Commons Attribution 4.0 International License, which permits use, sharing, adaptation, distribution and reproduction in any medium or format, as long as you give appropriate credit to the original author(s) and the source, provide a link to the Creative Commons licence, and indicate if changes were made. The images or other third party material in this article are included in the article's Creative Commons licence, unless indicated otherwise in a credit line to the material. If material is not included in the article's Creative Commons licence and your intended use is not permitted by statutory regulation or exceeds the permitted use, you will need to obtain permission directly from the copyright holder. To view a copy of this licence, visit <http://creativecommons.org/licenses/by/4.0/>.

© The Author(s) 2024